

## **A 8 GHz microwave substrate integrated waveguide power amplifier using complementary split ring resonators**

Dai Xuan Loi<sup>1\*</sup>, Luong Duy Manh<sup>2</sup>, Ta Chi Hieu<sup>2</sup>, Vu Le Ha<sup>1</sup>, Tran Van Toan<sup>3</sup>

<sup>1</sup>Academy of Military Science and Technology, 17 Hoang Sam, Cau Giay, Hanoi, Vietnam;

<sup>2</sup>Le Quy Don Technical University, 236 Hoang Quoc Viet, Bac Tu Liem, Hanoi, Vietnam.

<sup>3</sup>Air Defence-Air Force Academy, Kim Son, Son Tây, Hà Nội, Việt Nam.

\*Corresponding author: daixuanloi@gmail.com

Received 06 May 2024; Revised 27 Oct. 2024; Accepted 12 Dec. 2024; Published 25 Dec. 2024.

DOI: <https://doi.org/10.54939/1859-1043.j.mst.100.2024.31-38>

### **ABSTRACT**

*This paper introduces a design for a microwave substrate integrated waveguide (SIW) power amplifier (PA) for modern wireless communications. The amplifier design incorporates complementary split ring resonator (CSRR) structures integrated within the SIW to achieve low-loss characteristics and miniaturization through a below cut-off frequency operation approach. The designed PA operates at 8 GHz and exhibits good performance, which are measured output power  $P_{out}$  of 35.51 dBm, a maximum power added efficiency PAE of 47.2% and a power gain of 12.51 dB. The final circuit occupies just a compact size of  $41 \times 15.7 \text{ mm}^2$  benefiting from using the CSRR structure. The proposed PA employs a low-cost QFN packaged GaN HEMT device from Qorvo and it was designed and fabricated on a cost-effective RO4003C substrate. The simulated results agree well with the measured ones validating the accuracy of the design. With promising measured results, the proposed PA can be a potential candidate for using in the modern wireless communication systems.*

**Keywords:** Power amplifier (PA); Substrate integrated waveguide (SIW); Complementary split ring resonators (CSRR).

### **1. INTRODUCTION**

The emergence of Substrate Integrated Waveguide (SIW) technology represents a significant advancement in addressing the limitations inherent in microstrip technology, offering a compelling option for the development of modern microwave and millimeter-wave components. With its array of advantageous features including low-weight, low-cost, low-loss, high integration, and high-power capability [1], SIW technology has garnered substantial attention in the realm of microwave power amplifier design.

Recent studies [2, 3] have introduced innovative methodologies leveraging SIW technology for the creation of power amplifiers. One notable approach involves the integration of inductive metallized posts within the SIW input/output matching networks. Through strategic adjustment of these posts' positions, optimal impedance matching can be achieved. For instance, in [2], researchers utilized an inductive metallized post for impedance matching at 2.14 GHz, yielding impressive results with a high Power Added Efficiency (PAE) of 65.9% and an output power ( $P_{out}$ ) of 39.8 dBm. Moreover, in [3], authors expanded upon this concept by not only utilizing metallized posts for impedance transformation but also incorporating two stub resonators into the microstrip to SIW transitions. This combined integration facilitated the creation of an SIW bandstop filter, effectively suppressing the second harmonic and thereby enhancing the overall performance of the power amplifier system.

In the referenced papers [4-6], researchers introduce an innovative strategy employing iris-type input/output matching networks. Particularly noteworthy is the work presented in [5], where a Substrate Integrated Waveguide (SIW) power amplifier (PA) operated at a frequency of 8 GHz, delivering a power gain of 5.49 dB and achieving a remarkable Power Added Efficiency (PAE) of 29.38%. Moreover, in [7], authors proposed an alternative approach to designing SIW power

amplifiers by integrating complementary split ring resonators into the SIW input/output circuits. Notably, the SIW PA operated at a frequency of 6 GHz, exhibiting impressive performance characteristics with a high PAE of 57.05% and an output power ( $P_{out}$ ) of 37.43 dBm.

This paper introduces a novel SIW PA employing complementary split ring resonators in the SIW input/output matching networks. The SIW PA is designed to at 8 GHz, a critical band for X-band radio relay systems. To realize this design, the Qorvo GaN TGF2977-SM transistor is selected as the active element due to its renowned high efficiency and cost-effectiveness [8]. The parameters of the SIW structure, loaded by CSRR, are meticulously optimized to achieve optimal impedance matching and maximize efficiency. The PA was designed, simulated and tested for it both small-signal and large-signal performance.

## 2. POWER AMPLIFIER DESIGN

The schematic of the PA is shown in figure 1. The input/output circuit consists of an input/output bias circuit along with a SIW input/output matching circuit. Specifically, the SIW matching circuit is meticulously designed utilizing the complementary split ring resonators (CSRR) structure, strategically detuned to achieve optimal matching for both real and complex impedance. The positioning of the bias circuit between the transistor and the SIW matching circuit enables the SIW matching circuit to effectively mediate the transformation between the system impedance  $50 \Omega$  and the input impedance ( $Z_{in}$ ) or output impedance ( $Z_{out}$ ) of the bias circuit.

The Qorvo GaN HEMT TGF2977-SM transistor was chosen for its advantageous high efficiency. The transistor is biased in class AB operation with a gate supply voltage  $V_G$  of -2.76 V and a drain supply voltage  $V_D$  of 32 V. The large-signal model HMT\_QOR\_TGF2977\_SM\_001\_MDLXQorvoGaN utilized in this study is created by Modelithics [9]. Employing the Load Pull technique, the source impedance ( $Z_S$ ) and load impedance ( $Z_L$ ) at the fundamental frequency of 8 GHz were determined as  $22.505-j*40.782 \Omega$  and  $5.92+j*5.233 \Omega$ , respectively. The proposed PA is synthesized and designed using RO4003C substrate with dielectric constant 3.55, loss tangent 0.0027 and substrate height of 0.508 mm. All simulations are performed using Keysight ADS.

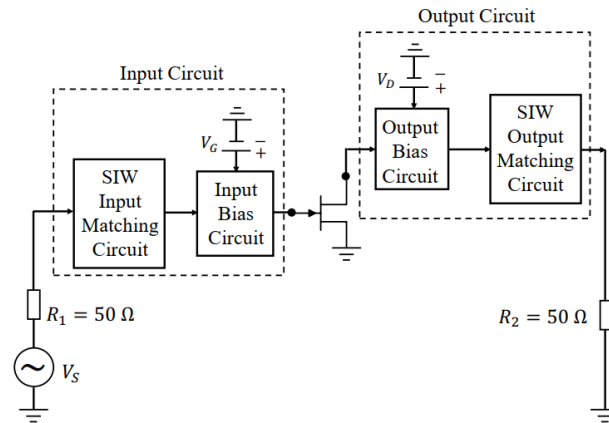


Figure 1. Block diagram of SIW PA.

### 2.1. Input matching circuit design

A schematic diagram of an input bias circuit is shown in figure 2. Within the figure,  $C_1=1.6 \text{ pF}$  represents an RF-bypass capacitor sourced from the Murata library version GJM0335C1E1R6BB01. Capacitor  $C_1$  serves the additional function of allowing RF signal transmission. Hence, it's chosen to have minimal impedance at 8 GHz. The bias line TL4 is configured as a quarter-wavelength ideal transmission line, precisely adjusted to present high

impedance at 8 GHz. In addition, the RF signal is shorted by a stub Stub1 to protect the dc source. TL1 operates as a 50-ohm transmission line, while TL3 facilitates connection to the transistor.

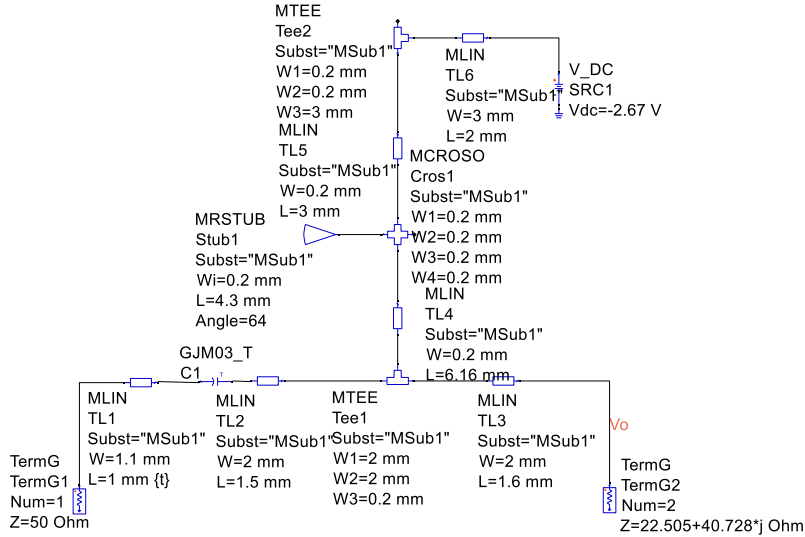


Figure 2. Schematic diagram of input bias circuit.

Figure 3 illustrates the proposed SIW input matching circuit featuring CSRR. The SIW structure is engineered to establish the cut-off frequency ( $f_c$ ) to enable evanescent mode operation, while the SIW taper is implemented to facilitate impedance matching between the standard 50  $\Omega$  transmission line and the SIW structure. It is imperative to design the taper with low loss to minimize losses during the transition from the 50  $\Omega$  line and the SIW structure. The CSRR is engraved on the top layer and consists of two rectangular split rings. The parameters of the CSRR are adjusted to achieve detuning for impedance transformation.

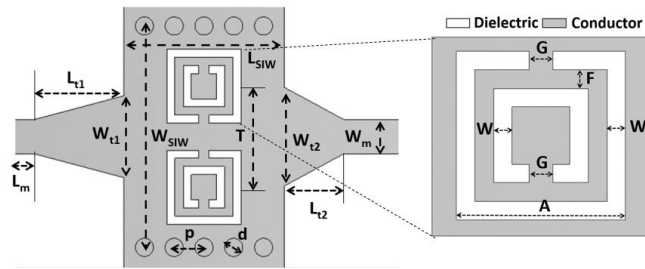


Figure 3. Structure of the SIW input matching circuit with CSRR.

Table 1 summarizes the detailed dimensions of the designed SIW input matching circuit with CSRR.

Table 1. Dimensions of the SIW input circuit.

$W_{t1}$ , mm	$W_{t2}$ , mm	$W_m$ , mm	$W_{SIW}$ , mm	$L_{SI}$ , mm	$L_{t1}$ , mm	$L_{t2}$ , mm	$L_m$ , mm	$A$ , mm	$W$ , mm	$F$ , mm	$G$ , mm	$T$ , mm	$d$ , mm	$P$ , mm
2.5	2.5	1.15	7.45	5.4	1.9	1.9	1.05	2.57	0.27	0.27	0.35	3.2	0.61	1

Figure 4 showcases the co-simulation diagram, illustrating the input circuit consisting of an SIW matching circuit and the input bias circuit. One terminal of the input bias circuit is the complex conjugate impedance  $Z_s$  ( $Z_s^* = 22.505 + j*40.782$ ).

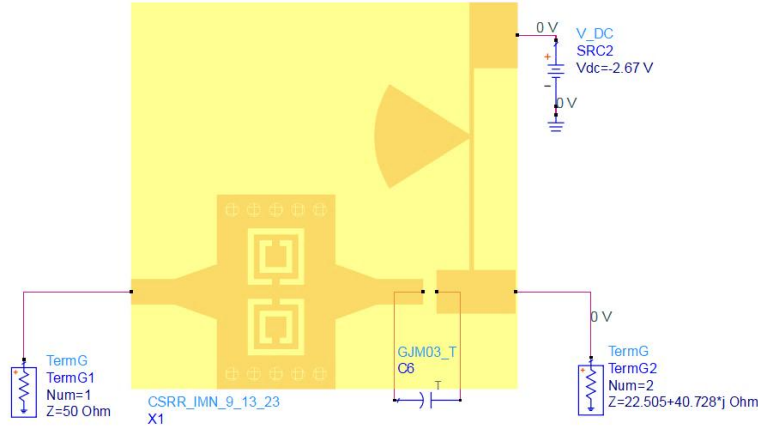


Figure 4. Co-simulation diagram of the input circuit.

Furthermore, the small signal characteristics of the input circuit's co-simulation are depicted in figure 5.a. At the 8 GHz frequency, the reflection coefficient S22 is -14.99 dB, while S11 is -14.46 dB. Additionally, the transmission coefficient S21 exhibits is value of -0.7 dB, showcasing a notable peak near the 8 GHz frequency.

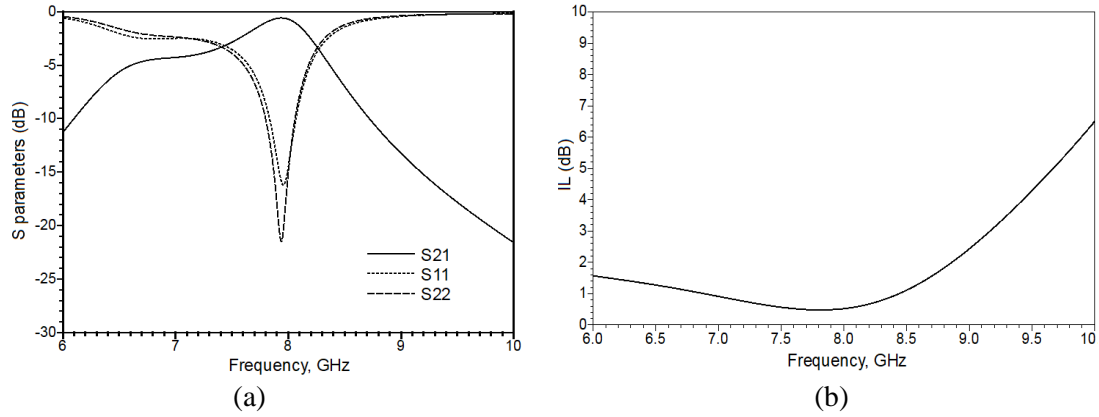


Figure 5. Small signal characteristics of the input circuit. (a) S-parameters; (b) Insertion loss.

Where S11 and S21 are the scattering parameters of the matching networks.

Finally, figure 5.b. describes the loss of the input circuit is relatively low at 8 GHz is 0.52 dB. Here the insertion loss (IL) of the matching networks is evaluated by the following formula:

$$IL (dB) = 10 \log_{10} \left( \frac{1 - |S_{11}^2|}{|S_{21}^2|} \right) \quad (1)$$

## 2.2. Output matching circuit design

Output circuit is designed in a similar way to the input circuit. Summaries of the detailed dimensions of the designed SIW output matching circuit with CSRR shown in table 2.

Table 2. Dimensions of the SIW output circuit.

W <sub>t1</sub> , mm	W <sub>t2</sub> , mm	W <sub>m</sub> , mm	W <sub>SIW</sub> , mm	L <sub>SIW</sub> , mm	L <sub>t1</sub> , mm	L <sub>t2</sub> , mm	L <sub>m</sub> , mm	A, mm	W, mm	F, mm	G, mm	T, mm	d, mm	P, mm
2.2	2.2	1.15	7.45	5.4	2.7	2.7	2	2.37	0.28	0.28	0.35	3.4	0.61	1

Figure 6.a. shows the co-simulation diagram of the output circuit. Within this diagram, RF-bypass capacitor C<sub>1</sub>=1.6 pF and all the dimensions of the output bias circuit are meticulously detailed in figure 6.b.

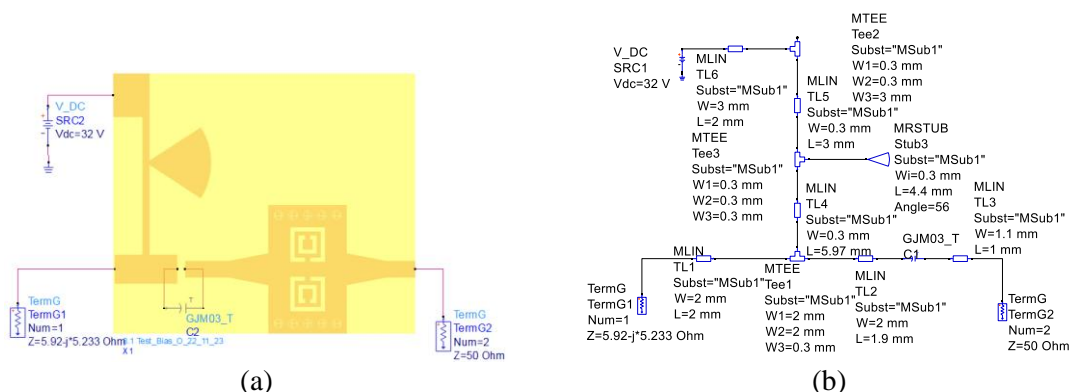


Figure 6. (a) Co-simulation diagram of the output circuit; (b) Schematic diagram of output bias circuit.

The small signal characteristics of the output circuit are presented in figure 7. At 8 GHz, the reflection coefficient S22 is -19.26 dB, S11 is -27.43 dB and transmission coefficient S21 is -0.52 dB, exhibiting a peak near the frequency of 8 GHz.

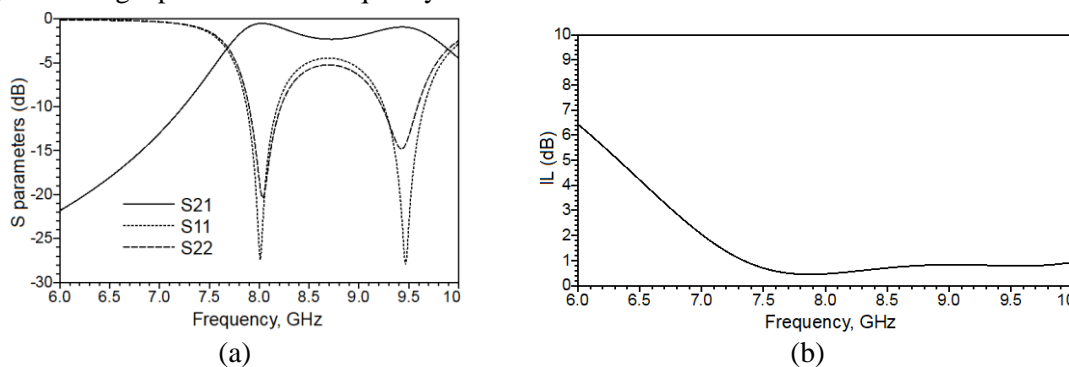


Figure 7. Small signal characteristics of the output circuit. (a) S-parameters; (b) Insertion loss.

Finally, figure 7.b. shows the loss of the input circuit is relatively low at 8 GHz is 0.46 dB.

### 3. IMPLEMENTATION AND EVALUATION OF THE PROPOSED PA

The co-simulation schematic and the fabricated propotype of the proposed PA are indicated in figure 8.a. and figure 8.b., respectively.

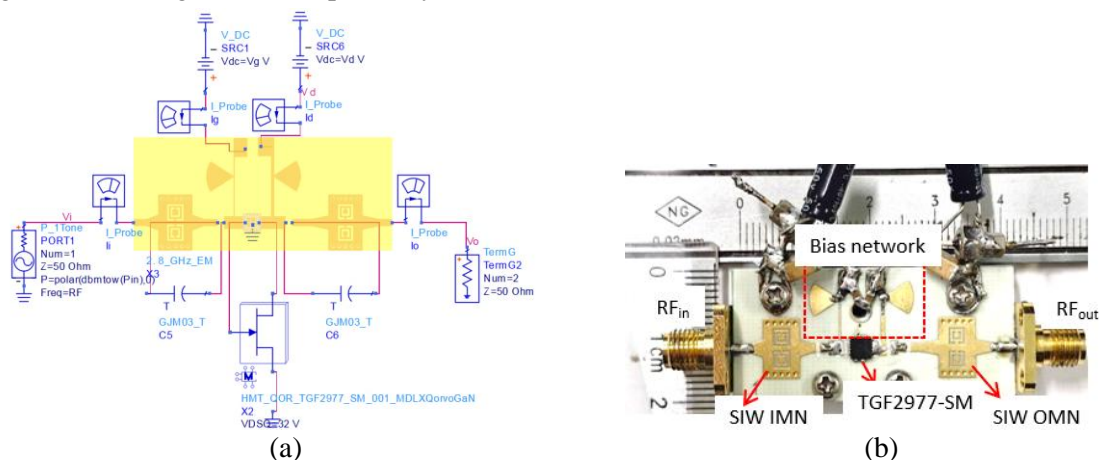
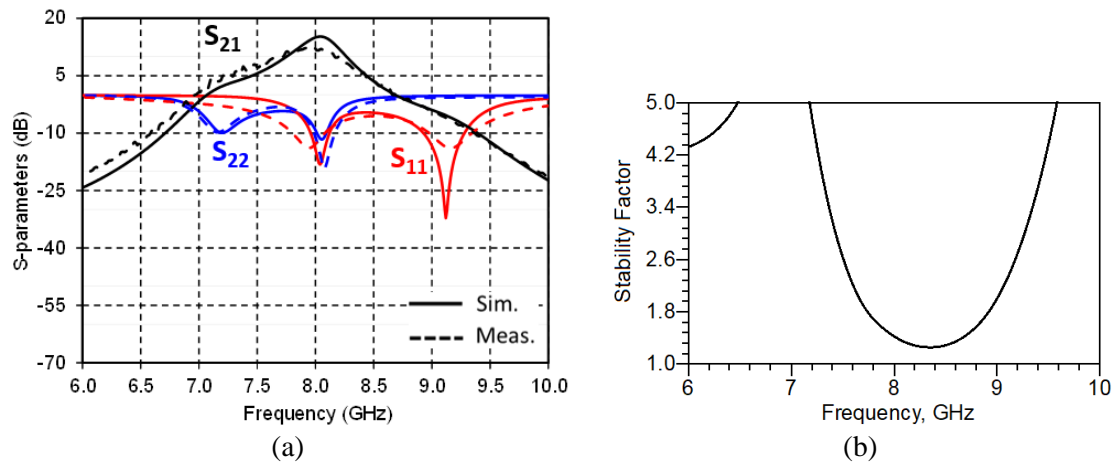


Figure 8. The proposed PA. (a) Co-simulation schematic of; (b) Fabricated propotype.

The PA was designed and simulated using a Keysight ADS 2019 simulator. The substrate used is a cost-effective Rogers RO4003C with a thickness of 0.508 mm, dielectric constant of 3.38, loss tangent of 0.0027 and conductor thickness of 1-oz. The bypass capacitors in the model series are identified as GQM1555C2DR75CB01, with a capacitance value of 0.75 pF. The DC gate voltage is set to  $V_G = -2.76$  V, while the DC drain voltage is maintained at  $V_D = 32$  V.

The proposed PA is then experimentally evaluated in both small-signal and large-signal characteristics. Figure 9.a. shows the simulated and measured S-parameters of the proposed PA. Specifically, the measured small-signal gain is 12.51 dB. In addition, the measured input return loss S11 is -13.4 dB, while the output return loss S22 is -10 dB, indicating a low return loss at the 8 GHz frequency.



**Figure 9.** (a) Simulated and measured small-signal performance of the proposed PA; (b) Stability response of the designed PA.

Figure 9.b. presents the stability factor of the PA. It can be seen that stability factor of the PA is 1.42 greater than the unity factor, indicating that the designed PA remains stable at the operating frequency of 8 GHz.

Figure 10 presents the experimental setup for evaluation of the large-signal performance of the proposed PA. Finally, the simulated and measured large signal characteristics of the proposed PA are shown in figure 11. It can be seen good agreements between simulations and measurements for the designed PA. The measured PAE, saturated output power and power gain are 47.2%, 35.57 dBm and 11.3 dB.

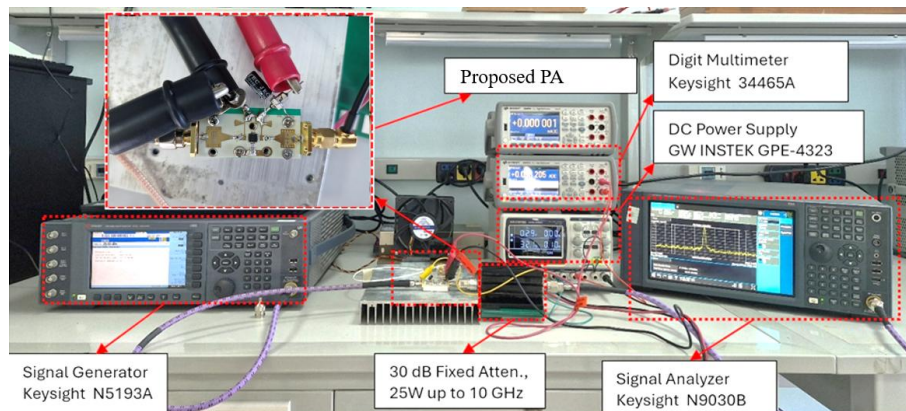


**Figure 10.** Experimental setup for evaluation of the large-signal performance of the proposed PA.

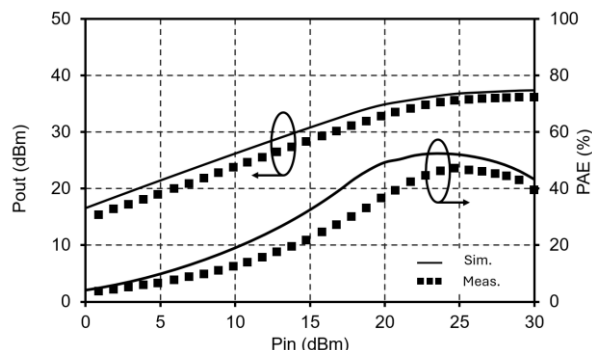


Figure 11. Simulated and measured large-signal performance of the proposed PA.

Table 3 provides a comparison between the designed PA and previous designs. The designed PA exhibits superior performance in terms of Pout and PAE at the frequency of 8 GHz. The size of the proposed power amplifier was decreased due to the implementation of the CSRR structure, resulting in a compact form factor of 41x15.7 mm.

Table 3. Comparisons with other previous SIW PA.

Ref.	Trans.	Freq. (GHz)	P <sub>out</sub> (dBm)	G (dB)	PAE (%)	Size (mm x mm)
[2]	Cree	2.18	39.8	-	65.9	101.6x 177.8
[3]	Cree	3.55	40.47	11.47	52.2	-
[4]	NEC	X-band	-	10	-	1.5 λ <sub>g</sub> (w ≈ 46)
[5]	Cree	10	35.42	5.49	29.38	78.54x41.89
[6]	Qorvo	6	37.43	13.43	57.05	74.18x28.42
<b>This work</b>	<b>Qorvo</b>	<b>8</b>	<b>35.57</b>	<b>11.3</b>	<b>47.2</b>	<b>41x15.7</b>

#### 4. CONCLUSIONS

This paper presents a SIW PA featuring CSRR in the matching circuits. The designed PA demonstrates commendable performance across both small signal and large signal levels. Notably, it exhibits favorable small signal characteristics, including a good measured input return loss of -13.4 dB, measured output return loss of -10 dB and a measured power gain of 12.51 dB. Furthermore, the measured PAE, output power are 47.2 and 35.57 dBm. The integration of SIW technology with the CSRR configuration enables seamless integration of the PA with planar components at high frequencies. Additionally, the PA achieves excellent performance in terms of PAE, Pout, and gain. These attributes render the PA well-suited for application in X-band radio relay systems.

#### REFERENCES

- [1]. D. X. Loi, L. D. Manh, T. C. Hieu and V. L. Ha, "A Compact, Low-loss and High Passband Ratio Substrate Integrated Waveguide Triplexer using Complementary Split Ring Resonators," 2023 International Conference on Advanced Technologies for Communications (ATC), Da Nang, Vietnam, pp. 239-243, (2023).
- [2]. Z. Wang and C. -W. Park, "Novel substrate integrated waveguide (SIW) type high power amplifier using Microstrip-to-SIW transition," Proc.2013 Asia-Pacific Microwave Conference Proceedings (APMC), (2013).
- [3]. D. T. J. Diatta and C. -W. Park, "Substrate integrated waveguide (SIW) power amplifier using SIW bandstop filter for harmonic control working at 3.55 GHz," Proc. 2020 IEEE Asia-Pacific Microwave Conference (APMC), (2020).

- [4]. M. Abdolhamidi and M. Shahabadi, "X-Band substrate integrated waveguide amplifier," IEEE Microwave and Wireless Components Letters, vol. 18, pp. 815–817, (2008).
- [5]. P. Pech, P. Kim, and Y. Jeong, "Microwave amplifier with substrate integrated waveguide bandpass filter matching network," IEEE Microwave and Wireless Components Letters, vol. 31, pp. 401–404, 2021.
- [6]. Y. Gao et al., "Substrate Integrated Waveguide Filter–Amplifier Design Using Active Coupling Matrix Technique," in IEEE Transactions on Microwave Theory and Techniques, vol. 68, no. 5, pp. 1706–1716, May (2020).
- [7]. H. T. T. Tran and L. D. Manh, "Microwave Substrate Integrated Waveguide Power Amplifier using Complementary Split Ring Resonators," 2023 International Conference on Advanced Technologies for Communications (ATC), Da Nang, Vietnam, pp. 269–274, (2023).
- [8]. S. Nakajima, "GaN HEMTs for 5G base station applications," Proc. 2018 IEEE International Electron Devices Meeting (IEDM), pp. 320–323, (2018).
- [9]. <https://www.modelithics.com/>

### TÓM TẮT

#### **Bộ khuếch đại công suất băng tần 8 GHz ứng dụng công nghệ ống dẫn sóng tích hợp chất nền sử dụng khung cộng hưởng kép**

Bài báo này trình bày thiết kế bộ khuếch đại công suất ứng dụng công nghệ ống dẫn sóng tích hợp chất nền (SIW) cho truyền thông không dây hiện đại. Bộ khuếch đại thiết kế bằng cách khoét hai khung cộng hưởng trên SIW để đạt được hệ số tổn hao thấp và thu nhỏ kích thước do khả năng hoạt động dưới tần số cắt dưới. Bộ khuếch đại công suất được thiết kế hoạt động ở tần số 8 GHz với hiệu suất tăng thêm (PAE) đo được là 47.2% với công suất đầu ra  $P_{out}$  là 35.57 dBm và hệ số khuếch đại công suất đạt được là 12.51 dB. Bộ khuếch đại đề xuất có kích thước nhỏ gọn  $41 \times 15.7 \text{ mm}^2$  nhờ sử dụng cấu trúc CSRR. Bộ khuếch đại sử dụng bóng bán dẫn GaN HEMT đóng gói QFN của hãng Qorvo có giá thành thấp và được chế tạo trên vật liệu phổ thông RO4003C. Các kết quả đo thực tế phù hợp với kết quả đo được cho thấy tính chính xác của giải pháp thiết kế. Với kết quả đo lường thực tế cho thấy bộ khuếch đại đề xuất hứa hẹn là ứng cử viên tiềm năng để sử dụng trong các hệ thống truyền thông không dây hiện đại.

**Từ khoá:** Bộ khuếch đại công suất (PA); Ống dẫn sóng tích hợp chất nền (SIW); Khung cộng hưởng kép (CSRR).